PNAS
www.pnas.org

Supplementary Information for

Specific Electromagnetic Radiation in the Wireless Signal Range Increases Wakefulness in Mice

Lingyu Liu[1,5], Hu Deng[2,1,5], Xiaping Tang[3,4,5], Yingxian Lu[1], Jiayao Zhou[1], Xiaofei Wang[1], Yanyu Zhao[3,4], Bing Huang[3,4], Yigong Shi[1,3,4]

[1]Beijing Advanced Innovation Center for Structural Biology & Frontier Research Center for Biological Structure, Tsinghua-Peking Joint Center for Life Sciences, School of Life Sciences, Tsinghua University, Beijing 100084, China

[2]Peking University HuiLongGuan Clinical Medical School, Beijing Huilongguan Hospital, Beijing 100096, China

[3]Westlake Laboratory of Life Sciences and Biomedicine, Xihu District, Hangzhou 310024, Zhejiang Province, China

[4]Key Laboratory of Structural Biology of Zhejiang Province, School of Life Sciences, Westlake University; Institute of Biology, Westlake Institute for Advanced Study, 18 Shilongshan Road, Hangzhou 310024, Zhejiang Province, China

[5]These authors contributed equally to this work.

Yigong Shi
Email: shi-lab@tsinghua.edu.cn

This PDF file includes:

Supplementary text
Figures S1 to S13
SI References

Supplementary Materials and Methods

Radiation equipment setup

A MXG Vector signal generator (Agilent, N5181A) in combination with an amplifier (Rflight, NTWPA-1025100) was used to generate 2.4 GHz EMR of three distinct patterns: Pulse64W, Pulse8W, and Conti8W (Figure S1*A*). The signal was emitted through a directional coupler and a horn antenna (HD-26SGAH20NZJ). Absorbing materials were fixed to the inner surface of the animal container to drastically reduce reflection (Figure S1*B*). The peak power entering the horn antenna was checked regularly using a spectrum analyzer (Rigol, DSA875) and was maintained at 48±1 dBm, 39±1 dBm and 39±1 dBm for the Pulse64W, Pulse8W and Conti8W regimens, respectively. The power densities at the mouse cage were measured using an electromagnetic field meter (Wavecontrol S.L. SMP2 with WPF18 probe). Following preheating of the instruments, the noise level in the recording chamber was measured using a digital sound level meter (Smart sensor, AS824). The average noise levels for the Control, Pulse8W, Pulse64W, and Conti8W groups were 70.1±1.1 dB, 69.1±0.5 dB, 70.9±0.4 dB, and 70.1±0.8 dB, respectively, over the course of 5 minutes. Mice in the Control and the three radiation groups were housed under the same environment and were treated in the same way except EMR exposure.

Animals

All adult C57BL/6 wild-type male mice (24±1 g, 6-10 weeks) were housed in an isolated ventilated cage barrier facility at Tsinghua University. The mice were maintained on a 12/12-hour light/dark cycle (ZT0: 10 a.m.) at a temperature of 22 to 26 ^{o}C with sterile pellet food and water ad libitum for at least 7 days for habitation. The laboratory animal facility has been

accredited by the Association for Assessment and Accreditation of Laboratory Animal Care International and the Institutional Animal Care. All the animal protocols applied in this study have been approved by the Animal Care and Use Committee of Tsinghua University.

Electrode implantation

The cranial electrodes in the skull and the intracranial electrodes are integrated, which is designed to simultaneously record electroencephalogram (EEG), electromyography (EMG) and local field potential (LFP) signals. The mouse was anesthetized with pentobarbital sodium (50 mg/kg) via intraperitoneal injection. The surgery was performed for each mouse. The cranial electrodes – four stainless steel 304 screws (diameter 1.4 mm, length 4 mm) – were anchored on the skull. Two right screws (coordinates, bregma: AP +1.50 mm, ML +1.50 mm; AP -3.50 mm, ML +4.00 mm) were winded using silver wires as the reference or ground wire and two left screws (coordinates, bregma: AP +1.50 mm, ML -1.50 mm; AP -3.50 mm, ML -3.00 mm) (*1*) were winded using enameled copper wires to record EEG (*2, 3*). The EMG electrode wires were embedded under the trapezius muscles of mouse neck. The implanted intracranial electrode tungsten wire (A-M systems, 795500#) has a bare diameter of 50.8 μm and a coated diameter of 101.6 μm. The tips of the tungsten electrode wire were positioned to collect signals from the hippocampus (coordinates, bregma: AP -2.00 mm, ML +1.50 mm, DV -2.00 mm), vlPAG (coordinates, bregma: AP -4.60 mm, ML +0.60 mm, DV -2.60 mm), and PPT (coordinates, bregma: AP -4.60 mm, ML +1.20 mm, DV -3.40 mm). The electrodes and screws were fixed to the skull with dental cement. The mice used in the second sets experiments have only cranial electrodes, but not the intracranial electrodes.

Polysomnographic recording and data analysis

EEG, EMG and LFP signals were collected using a digital headstage (CerePlex μ). The data acquisition system (CerePlex Direct) receives the digital signal via flexible cables at a sample rate of 1000 Hz. All data were amplified and filtered (EEG, motion acceleration and LFP: low-pass 250 Hz, EMG: band-pass 10-250 Hz). All Video signals (STC-MB33USB) were monitored as an auxiliary method to determine the status of mouse sleep.

Using the sleep analysis software (SleepSign for animals, Kissei Comtec), we carried out spectral analysis of the filtered EEG data (band-pass 0.5-100 Hz) using fast Fourier transformation (FFT). The spectral signatures of EEG, EMG and acceleration signals were used to automatically score brain states into wakefulness, NREM and REM for each 4-second epoch according to the standard criteria (*4*). The scoring results were validated visually and corrected manually if necessary. The state classifications were verified by investigators who were blinded to the animal identity and experimental manipulations.

LFP spectrograms for consecutive 4 s epochs were estimated via a fast Fourier transformation of the filtered LFP data (band-pass 0.5-40 Hz) using a sliding window of 4 s length. The absolute LFP power density was normalized for each brain area (Hippocampus, vlPAG and PPT). Methods of normalization and removing artifacts followed the previous study (*4*). We also performed the same analysis in other frequency ranges such as 0-100 Hz. The results are similar to those of 0.5-40 Hz range.

Statistical analysis

All results are presented as the means ± standard error of the mean (SEM). The total amount of time for each state at three points (Pre/Pos1/Pos9) were compared between different radiation regimens using two-way repeated measures ANOVA with Bonferroni post-hoc comparisons. To quantify the degree of effect on sleep behavior caused by radiation, we computed the Radiation Effect Index (REI). REI of different radiation regimens were compared to 0 using one-sample *t* tests (two-tailed). Also, REI at different points (Pos1/Pos9) between different radiation regimens were compared using two-way repeated measures ANOVA with Bonferroni post-hoc comparisons. In order to confirm the normal sleep behavior of mouse, the difference of Pre data between control and other groups were compared using one-way ANOVA analysis with Bonferroni post-hoc comparisons. All statistical analyses were performed using SPSS 20.0 and Matlab.

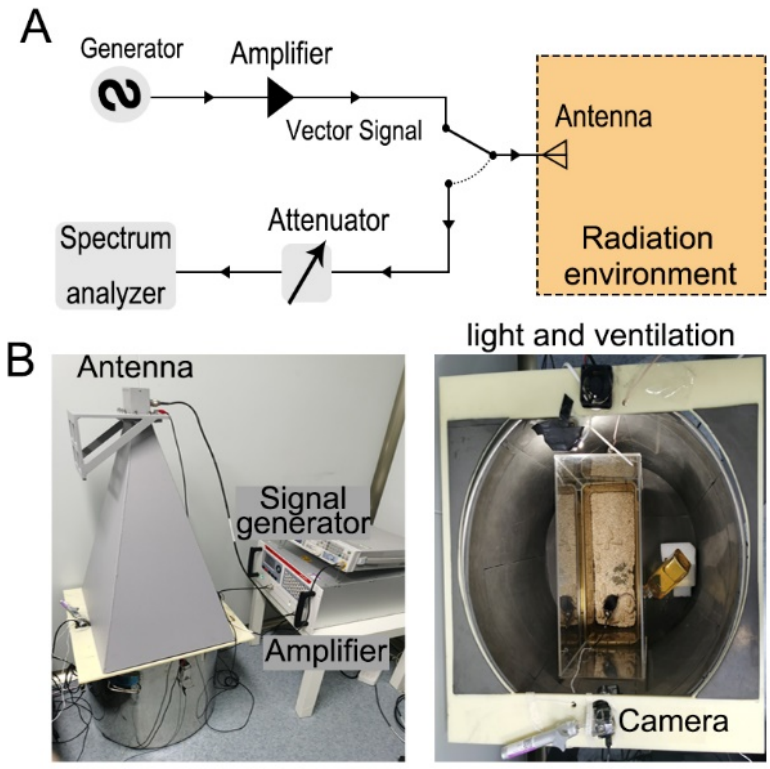

Fig. S1. Schematic diagrams of the experimental setup. (*A*) A schematic diagram of the circuit for EMR signals. A vector signal generator is combined with an amplifier to generate the three radiation regimens: Conti8W, Pulse8W, and Pulse64W. The EMR is then emitted through a horn antenna. The EMR power is checked by a spectrum analyzer to ensure the radiation intensity. (*B*) Photographs of the actual experimental setup. The overall setup (*Left*) and the mouse cage (*Right*) are shown here.

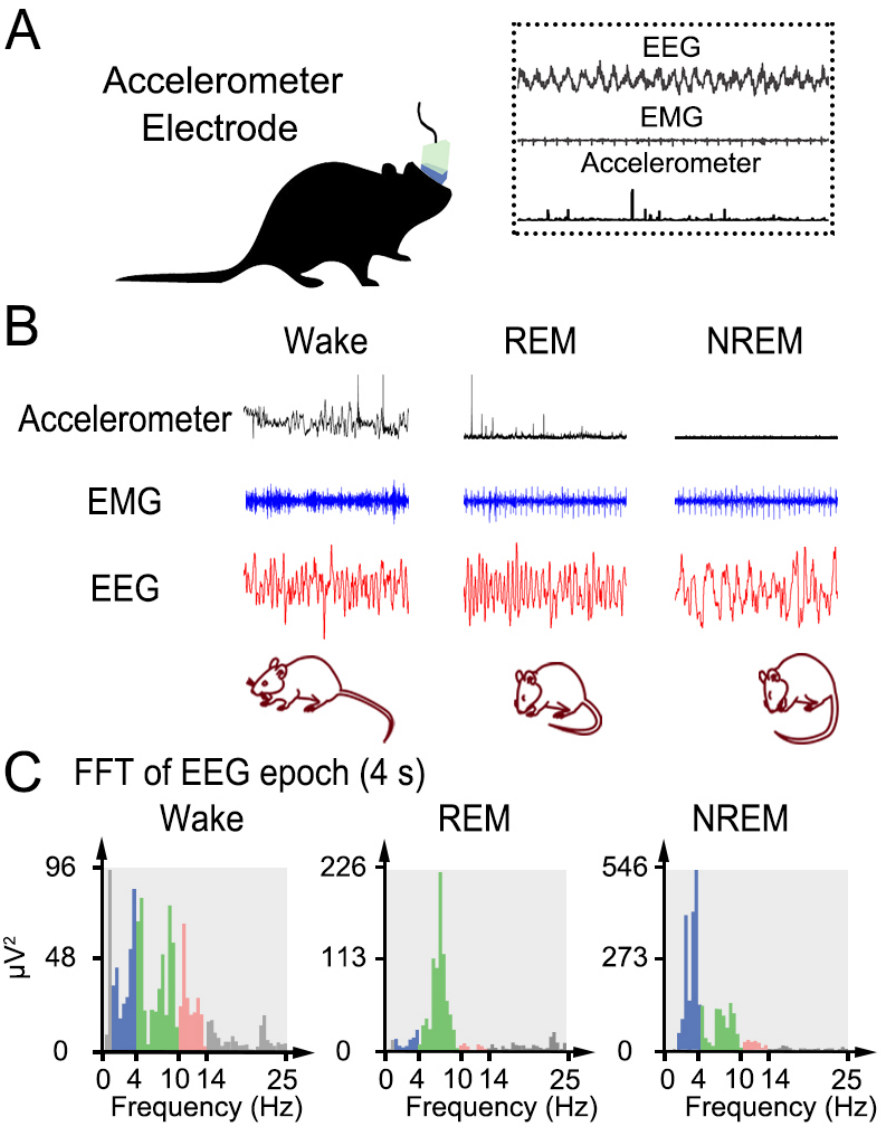

Fig. S2. Schematic diagrams of data recording and sleep behavior analysis. (*A*) A schematic diagram of data recording. The EEG, EMG and motion data are collected through the cranial electrodes, musculature electrodes, and accelerometer on the head stage, respectively. (*B*) Sleep behavior is reflected by characteristic waveforms of the EEG, EMG, and motion-accelerometer data. Shown are such characteristic waveforms for wakefulness, REM sleep, and NREM sleep. (*C*) Fast Fourier Transformation (FFT) of representative raw EEG data for wakefulness, REM sleep and NREM sleep in a 4-second epoch at the frequency range of 0-25Hz.

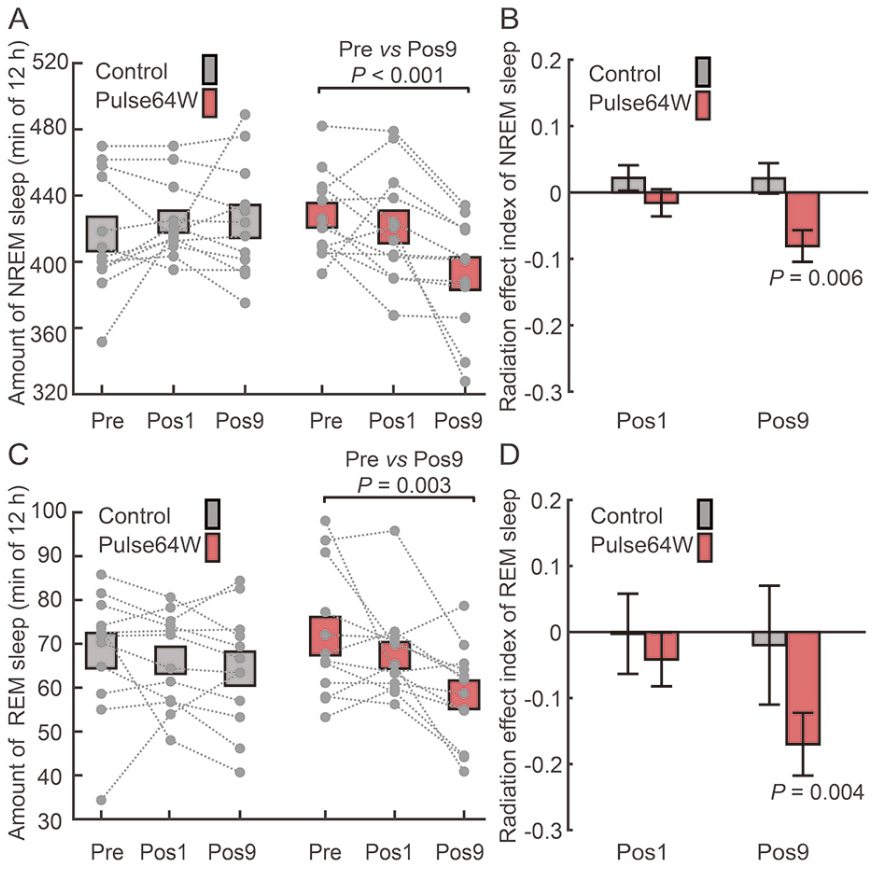

Fig. S3. The effect of the Pulse64W regimen on NREM and REM sleep. (*A*) A scatter plot of the NREM sleep for individual mouse. Each dot in the plot represents the total time of NREM sleep for one mouse, and the dotted line connects the data for the same mouse. The data shown here are for the Control and Pulse64W groups at Pre, Pos1, and Pos9. (*B*) Evaluation of the change of NREM sleep through analysis of the radiation effect index (REI). This analysis shows statistically significant decrease of NREM sleep at Pos9 for the Pulse64W group. (*C*) A scatter plot of the total time of REM sleep for individual mouse. (*D*) Evaluation of the change of REM sleep through analysis of the REI. This analysis shows statistically significant decrease of REM sleep at Pos9 for the Pulse64W group. n = 12 per group.

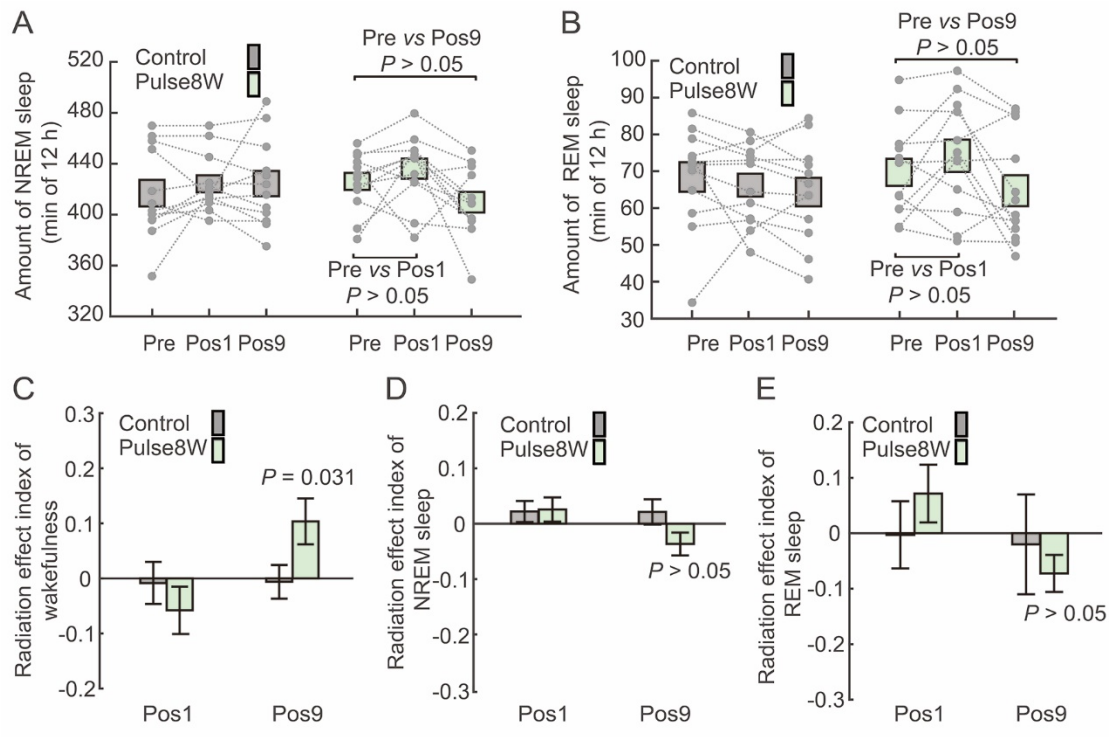

Fig. S4. The effect of the Pulse8W regimen on NREM and REM sleep. (*A*) A scatter plot of the NREM sleep for individual mouse. Each dot in the plot represents the total time of NREM sleep for one mouse, and the dotted line connects the data for the same mouse. The data shown here are for the Control and Pulse8W groups at Pre, Pos1, and Pos9. (*B*) A scatter plot of the total time of REM sleep for individual mouse. (*C*) Evaluation of wakefulness change through REI analysis. This analysis shows statistically significant change of wakefulness at Pos9 for the Pulse8W group. (*D*) Evaluation of the NREM sleep change through analysis of the REI. This analysis shows statistically insignificant change of NREM sleep at Pos9 for the Pulse8W group. (*E*) Evaluation of the REM sleep change through analysis of the REI. This analysis shows statistically insignificant change of REM sleep for the Pulse8W group. *n* = 12 per group.

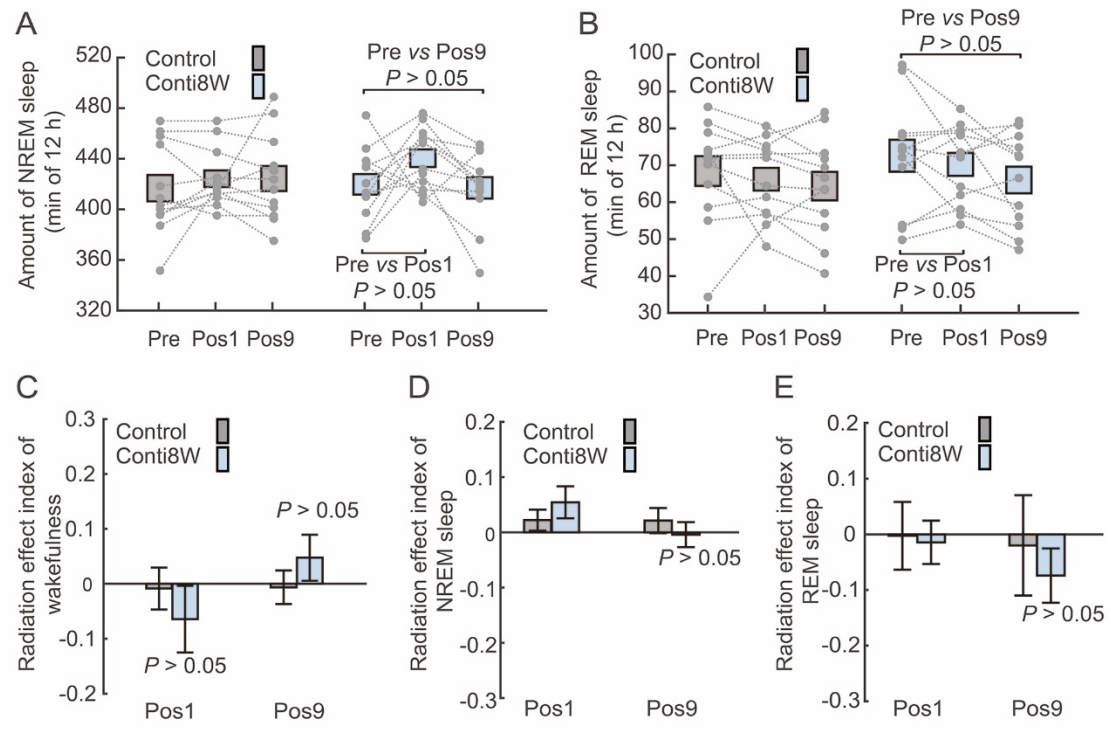

Fig. S5. The effect of the Conti8W regimen on NREM and REM sleep. (*A*) A scatter plot of the NREM sleep for individual mouse. Each dot in the plot represents the total time of NREM sleep for one mouse, and the dotted line connects the data for the same mouse. The data shown here are for the Control and Conti8W groups at Pre, Pos1, and Pos9. (*B*) A scatter plot of the total time of REM sleep for individual mouse. (*C*) Evaluation of wakefulness change through analysis of the REI. This analysis shows no statistically significant change of wakefulness at Pos9 for the Conti8W group. (*D*) Evaluation of the NREM sleep change through analysis of the REI. This analysis shows no statistically significant change of NREM sleep at Pos9 for the Conti8W group. (*E*) Evaluation of the REM sleep change through analysis of the REI. This analysis shows statistically insignificant change of REM sleep for the Conti8W group. n = 12 per group.

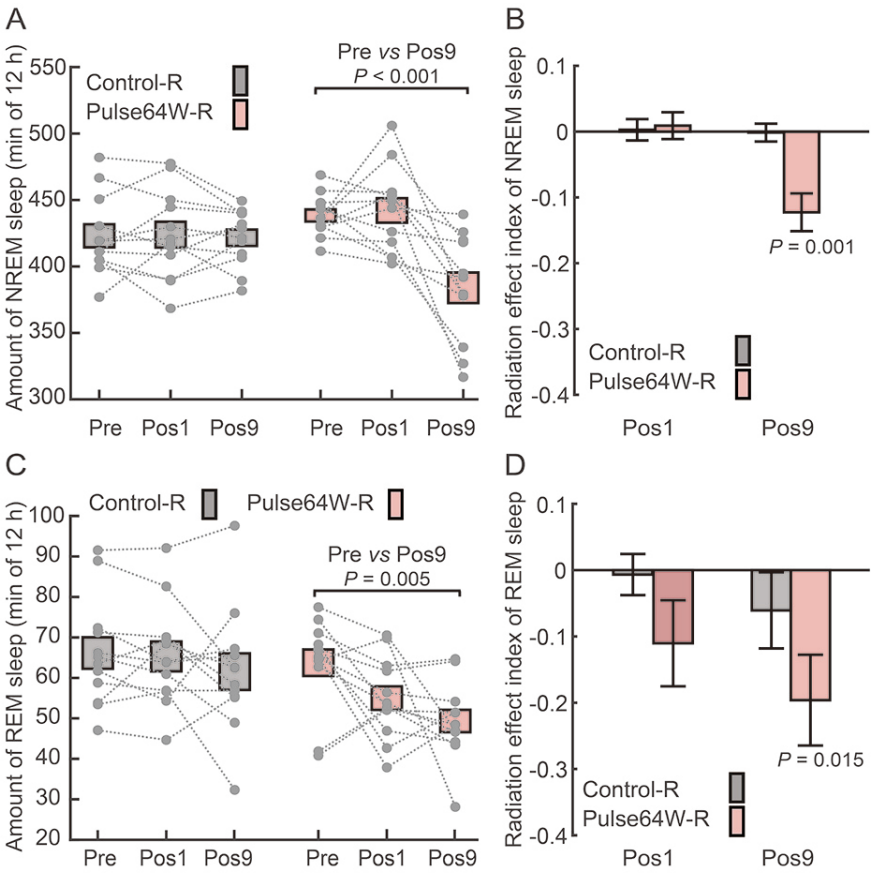

Fig. S6. Confirmation of the effect of Pulse64W on NREM and REM sleep using mice with only cranial electrodes. (*A*) A scatter plot of the NREM sleep for individual mouse. Each dot in the plot represents the total time of NREM sleep for one mouse, and the dotted line connects the data for the same mouse. (*B*) Evaluation of the NREM sleep change through analysis of the REI. This analysis shows statistically significant decrease of NREM sleep time at Pos9 for the Pulse64W-R group. (*C*) A scatter plot of the total time of REM sleep for individual mouse. (*D*) Evaluation of the REM sleep change through analysis of the REI. This analysis shows statistically significant decrease of REM sleep at Pos9 for the Pulse64W-R group. n = 12 per group.

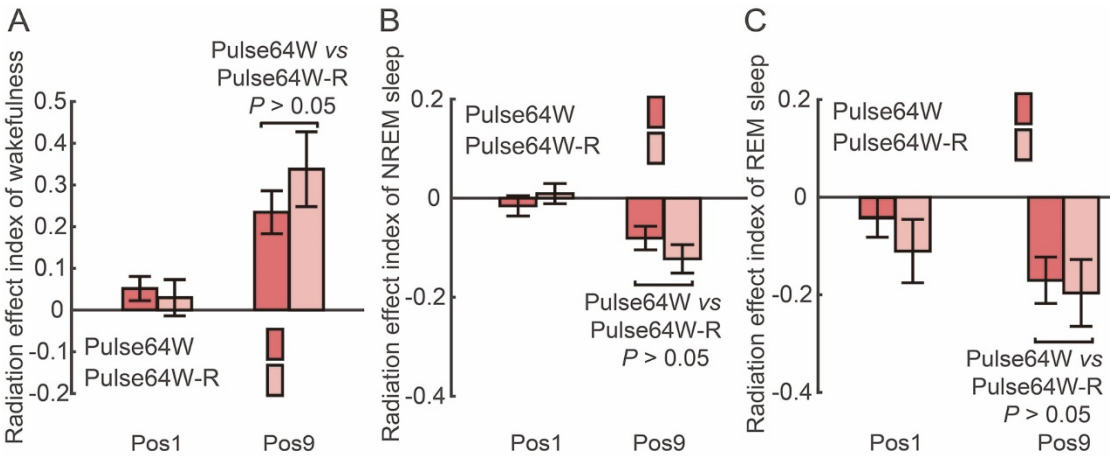

Fig. S7. Comparison of the REI results between the Pulse64W and Pulse64W-R groups. (*A*) Comparison of the REI results on the wakefulness between the Pulse64W and Pulse64W-R groups. This analysis reveals no significant change of REI on the wakefulness at Pos9 between the Pulse64W and Pulse64W-R groups. (*B*) Comparison of the REI on the NREM sleep between the Pulse64W and Pulse64W-R groups. This analysis reveals no significant change of REI on the NREM sleep at Pos9 between the Pulse64W and Pulse64W-R groups. (*C*) Comparison of the REI on the REM sleep between the Pulse64W and Pulse64W-R groups. This analysis reveals no significant change of REI on the REM sleep at Pos9 between the Pulse64W and Pulse64W-R groups. n = 12 per group.

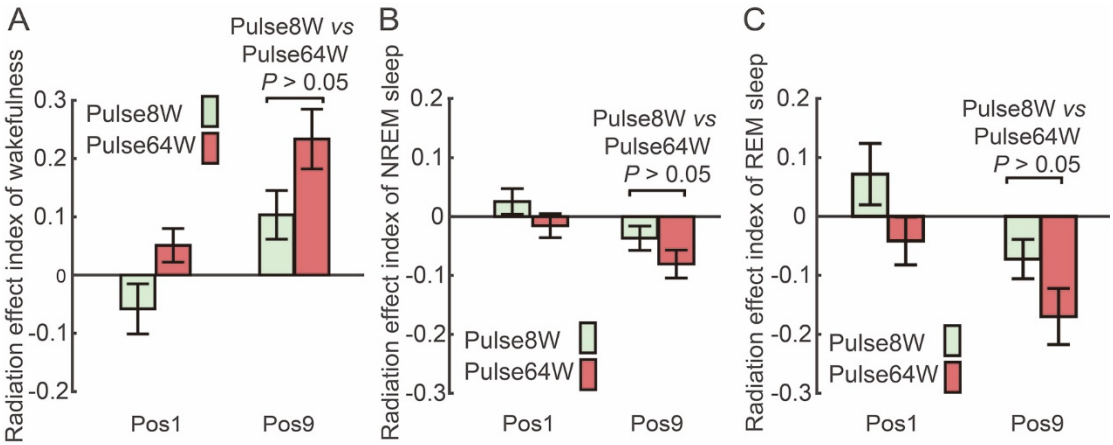

Fig. S8. Comparison of the effects on sleep behavior between the Pulse8W and Pulse64W regimens. (*A*) Comparison of the REI on the wakefulness between the Pulse8W and Pulse64W regimens. (*B*) Comparison of the REI on the NREM sleep time between the Pulse8W and Pulse64W regimens. (*C*) Comparison of the REI on the REM sleep time between the Pulse8W and Pulse64W regimens. n = 12 per group.

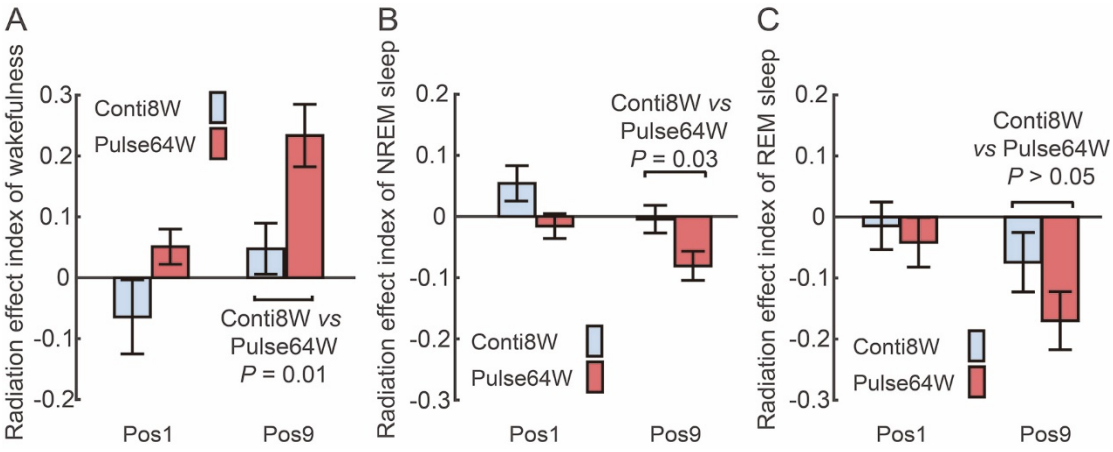

Fig. S9. Comparison of the effects on sleep behavior between the Conti8W and Pulse64W treatments. (*A*) Comparison of the REI on the wakefulness between the Conti8W and Pulse64W groups. This analysis reveals statistically significant increase of wakefulness at Pos9 for the Pulse64W group over that of the Conti8W group. (*B*) Comparison of the REI on the NREM sleep between the Conti8W and Pulse64W groups. This analysis reveals statistically significant decrease of NREM sleep at Pos9 for the Pulse64W group over that of the Conti8W group. (*C*) Comparison of the REI on the REM sleep between the Conti8W and Pulse64W groups. This analysis reveals statistically insignificant decrease of REM sleep at Pos9 for the Pulse64W group over that of the Conti8W group. n = 12 per group.

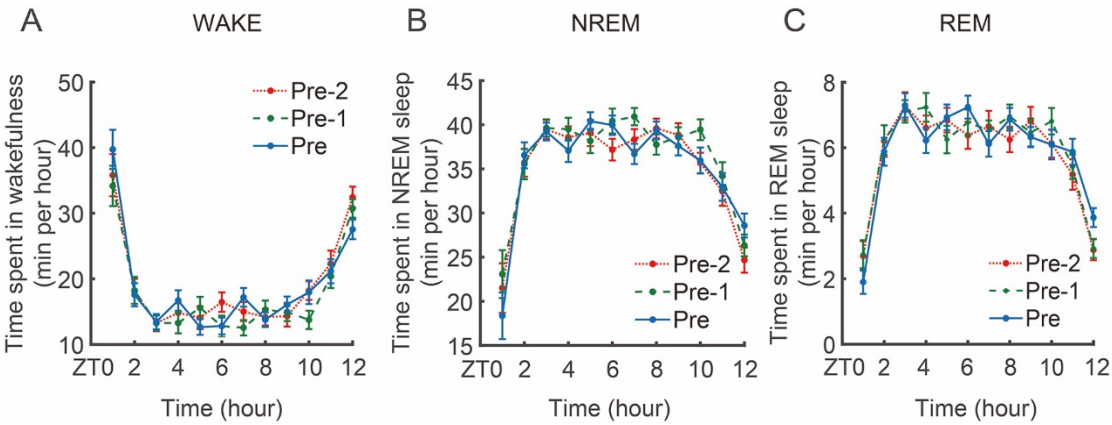

Fig. S10. Confirmation of normal sleep behavior. (*A*) The average time (in minutes) per hour spent in wakefulness during the 12-hour light phase at Pre-2, Pre-1, and Pre. Day –3 and Day –2 are referred to as “Pre-2” and “Pre-1”, respectively. The data for all 48 mice in the first sets of experiment were used for this analysis. (*B*) The average time (in minutes) per hour spent in NREM sleep during the 12-hour light phase at Pre-2, Pre-1, and Pre. (*C*) The average time (in minutes) per hour spent in REM sleep during the 12-hour light phase at Pre-2, Pre-1, and Pre.

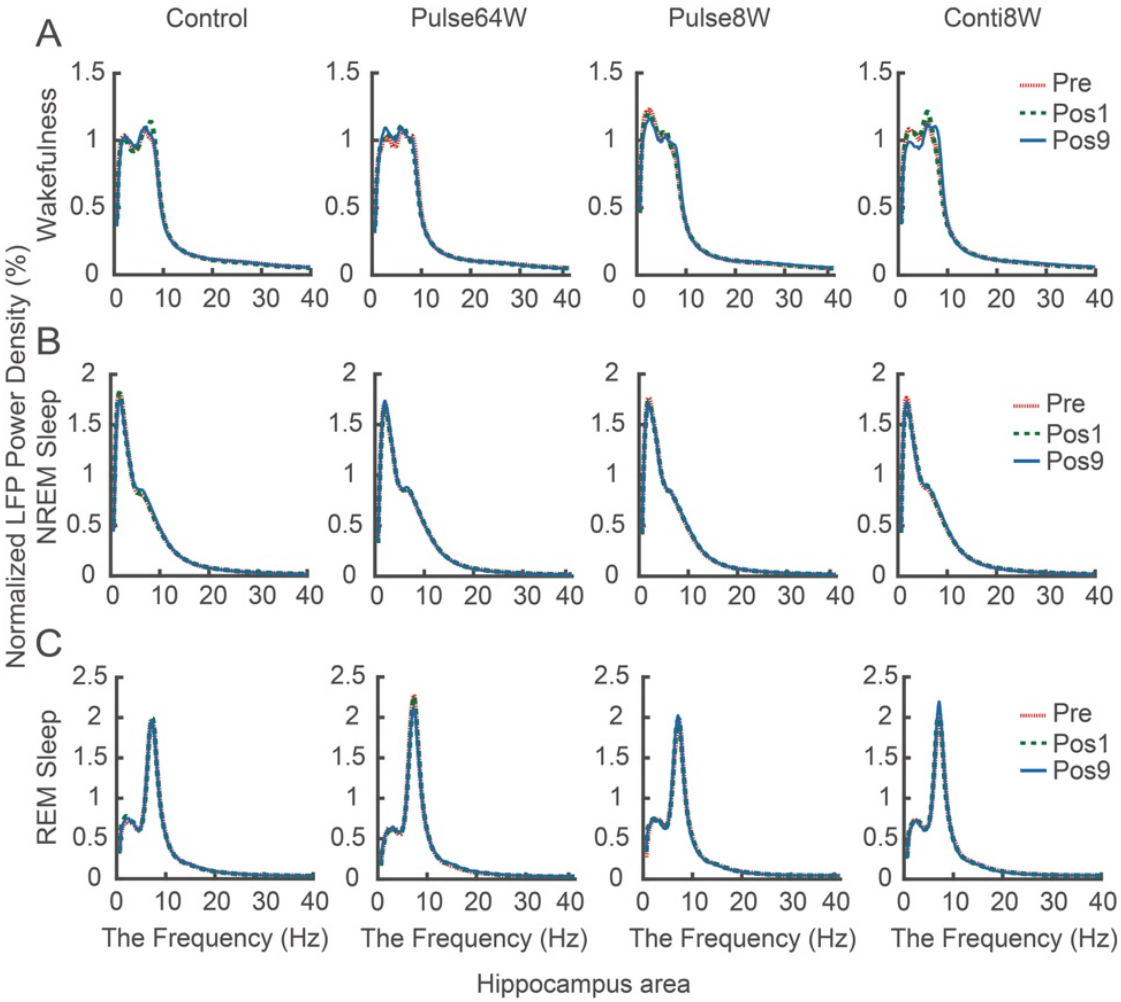

Fig. S11. Normalized LFP power density during wakefulness, NREM sleep and REM sleep in the hippocampus area. (*A*) The average normalized LFP power density during wakefulness in the hippocampus area at Pre (red), Pos1 (green) and Pos9 (blue). The data is shown for the Control group, Pulse64W group, Pulse8W group and Conti8W group (from left to right). (*B*) The average normalized LFP power density during NREM sleep in the hippocampus area at Pre (red), Pos1 (green) and Pos9 (blue). (*C*) The average normalized LFP power density during REM sleep in the hippocampus area at Pre (red), Pos1 (green) and Pos9 (blue).

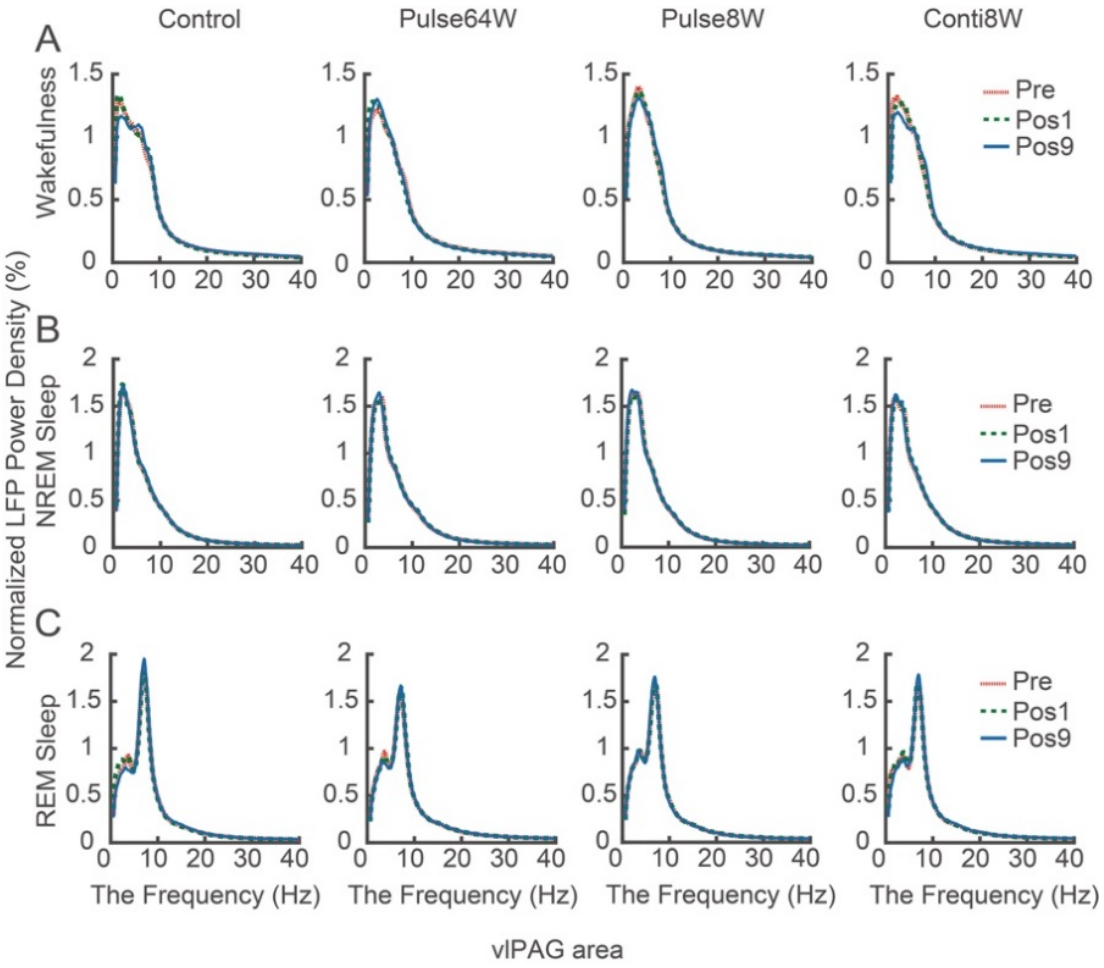

Fig. S12. Normalized LFP power density during wakefulness, NREM sleep and REM sleep in the vlPAG area. (*A*) The average normalized LFP power density during wakefulness in the vlPAG area at Pre (red), Pos1 (green) and Pos9 (blue). The data is shown for the Control group, Pulse64W group, Pulse8W group and Conti8W group (from left to right). (*B*) The average normalized LFP power density during NREM sleep in the vlPAG area at Pre (red), Pos1 (green) and Pos9 (blue). (*C*) The average normalized LFP power density during REM sleep in the vlPAG area at Pre (red), Pos1 (green) and Pos9 (blue).

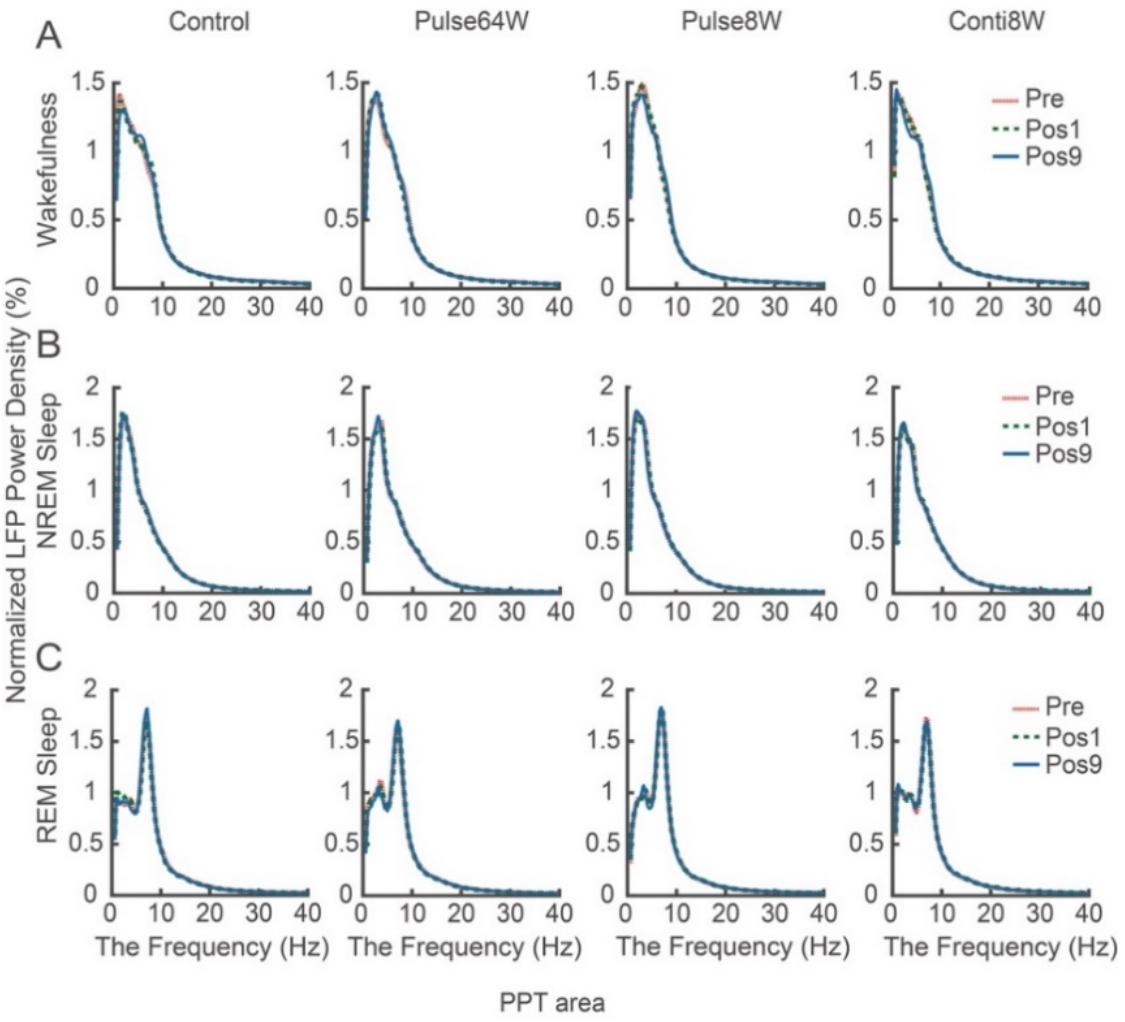

Fig. S13. Normalized LFP power density during wakefulness, NREM sleep and REM sleep in the PPT area. (*A*) The average normalized LFP power density during wakefulness in the PPT area at Pre (red), Pos1 (green) and Pos9 (blue). The data is shown for the Control group, Pulse64W group, Pulse8W group and Conti8W group (from left to right). (*B*) The average normalized LFP power density during NREM sleep in the PPT area at Pre (red), Pos1 (green) and Pos9 (blue). (*C*) The average normalized LFP power density during REM sleep in the PPT area at Pre (red), Pos1 (green) and Pos9 (blue).

References

1. K. Franklin, G. Paxinos, *The mouse brain in stereotaxic coordinates*. (Academic Press, 2008), vol. 3.
2. M. Xu *et al.*, Basal forebrain circuit for sleep-wake control. *Nature Neuroscience* **18**, 1641-1647 (2015).
3. K.-S. Chen *et al.*, A Hypothalamic Switch for REM and Non-REM Sleep. *Neuron* **97**, 1168-1176.e1164 (2018).
4. S. C. Ren *et al.*, The paraventricular thalamus is a critical thalamic area for wakefulness. *Science* **362**, 429-434 (2018).